OPEN ACCESS
Journal of Innovative Optical Health Sciences
Vol. 16, No. 4 (2023) 2250039 (11 pages)

DOI: 10.1142/S1793545822500390

World Scientific
www.worldscientific.com

A novel α-ketoamide reactivity-based two-photon fluorogenic probe for visualizing peroxynitrite in Parkinson's disease models

Tao Shao*, Xianning Xu*, Lan Wang†, Yu Shen*, Jun Zhao*, Huizi Li‡, Duoteng Zhang§, Wei Du†, Hua Bai*,¶,††, Bo Peng*,‖,†† and Lin Li*,†,§,**,††

*Frontiers Science Center for Flexible Electronics
Xi'an Institute of Flexible Electronics (IFE) and Xi'an Institute of Biomedical Materials & Engineering, Northwestern Polytechnical University
Xi'an 710072, P. R. China

†Key Laboratory of Flexible Electronics (KLOFE) & Institute of Advanced Materials (IAM)
Nanjing Tech University (NanjingTech), Nanjing 211816, P. R. China

‡Department of Outpatient
PLA Rocket Force Characteristic Medical Center
Beijing 100088, P. R. China

§The Institute of Flexible Electronics (IFE, Future Technologies)
Xiamen University, Xiamen 361005, Fujian, P. R. China

¶iamhbai@nwpu.edu.cn
‖iambpeng@nwpu.edu.cn
**iamlli@nwpu.edu.cn

Received 18 October 2022
Accepted 9 December 2022
Published 9 January 2023

Peroxynitrite ($ONOO^-$) contributes to oxidative stress and neurodegeneration in Parkinson's disease (PD). Developing a peroxynitrite probe would enable *in situ* visualization of the overwhelming $ONOO^-$ flux and understanding of the $ONOO^-$ stress-induced neuropathology of PD. Herein, a novel α-ketoamide-based fluorogenic probe (**DFlu**) was designed for $ONOO^-$ monitoring in multiple PD models. The results demonstrated that **DFlu** exhibits a fluorescence turn-on response to $ONOO^-$ with high specificity and sensitivity. The efficacy of **DFlu** for intracellular $ONOO^-$ imaging was demonstrated systematically. The results showed that **DFlu** can successfully visualize endogenous and exogenous $ONOO^-$ in cells derived from chemical and biochemical routes. More importantly, the two-photon excitation ability of **DFlu** has been well demonstrated by monitoring exogenous/endogenous $ONOO^-$ production and scavenging in live

††Corresponding authors.

zebrafish PD models. This work provides a reliable and promising α-ketoamide-based optical tool for identifying variations of $ONOO^-$ in PD models.

Keywords: α-Ketoamide; two-photon fluorogenic probe; bioimaging; peroxynitrite; Parkinson's disease.

1. Introduction

Parkinson's disease (PD) is a common neurodegenerative disorder with a high incidence in people over 65.[1–3] The functional loss of dopaminergic neurons in the substantia nigra is considered as the pathogenesis of PD.[4,5] Despite great efforts in the last few decades, it is difficult to insight the pathway of the loss of dopaminergic neurons.[6–8] Recent evidence indicates that abnormal levels of reactive oxygen species (ROS) can cause oxidative stress and induce DA neuronal degeneration during the pathogenesis of PD.[9,10] In addition, ROS overproduction is closely relative to other PD pathogenic factors, including mitochondrial dysfunction, inflammation and metal dyshomeostasis.[11,12] Therefore, exploring the role of elevated ROS level-induced neurotoxicity in PD is beneficial for early diagnosis and treatment.

Peroxynitrite ($ONOO^-$), a common ROS, is produced via the diffusion-limited coupling superoxide radical ($O_2^{\bullet-}$) and radical nitric oxide ($NO^{\bullet-}$).[13] Normal concentrations of $ONOO^-$ can maintain the redox balance and act as secondary messengers to regulate several pivotal signal-transduction pathways in cells.[14] On the contrary, excess $ONOO^-$ levels can lead to oxidative stress because of the strong oxidizing and nitrification ability in living biological systems.[15] Under such oxidative stress, lipids, nucleic acids, enzymes and proteins were changed in structure and function.[16] Ultimately, the disorders of biomolecular function result in severe PD disease.[17–19] From this point of view, $ONOO^-$ can be used as a PD biomarker. Thus, developing forceful tools to monitor the levels of $ONOO^-$ is beneficial for understanding the relationship between PD and $ONOO^-$ and for early diagnosis of PD.

At present, some methods have been exploited to detect $ONOO^-$ including electrochemical, electron spin resonance, liquid chromatography-mass spectrometry and fluorescence approaches.[20] Compared to the other techniques, fluorogenic probe-based detection are noninvasive and sensitive, which is ideal for monitoring $ONOO^-$ levels in biological systems.[21–25] Consequently, many $ONOO^-$ fluorogenic probes have been exploited relying on different recognition moieties, such as aryl boronic, aryl borate ester, N-aminophenol, trifluorocarbonyl, α-ketoamide and so on.[18,26–28] Among them, α-ketoamide has been widely used to detect the $ONOO^-$ levels in cardiovascular and hepatotoxicity disease models via combined inhibition of internal charge transfer (ICT) and photo-induced electron transfer (PET).[29] However, the α-ketoamide-based $ONOO^-$ fluorescence probe to track $ONOO^-$ fluctuations in the PD model has not been reported. Moreover, the existing α-ketoamide-based $ONOO^-$ fluorescence probes utilize aryl dicarbonyl which contains an electron-withdrawing substituent ($-NO_2$ or $-CN$) to increase the activity of α-ketoamide reaction with $ONOO^-$.[30] As the reactivity increases, other reactive species may interfere with the selective detection of $ONOO^-$, including H_2O_2 and ClO^-, which limits its application.[31,32] Therefore, developing a novel α-ketoamide-based recognition moiety with excellent selectivity toward $ONOO^-$ in PD model remains a challenge.

In this work, we designed a new α-ketoamide recognized group without 4-nitrophenyl aryl dicarbonyl construction unit to detect $ONOO^-$. Moreover, given the advantages of two-photon imaging technology in monitoring abnormal ROS-level *in vivo* models associated with PD models (Table S1), we employed naphthylamine ketone (**Flu**) as the two-photon fluorophore owing to its desirable two-photon action cross-section.[17,18,33–39] Ultimately, a non4-nitrophenyl aryl dicarbonyl α-ketoamide reactivity-based two-photon $ONOO^-$ fluorogenic probe (**DFlu**) was developed. The systematical investigation of photophysical properties demonstrated that the **DFlu** possesses excellent selectivity and suitable two-photon fluorescence intensity towards $ONOO^-$. *In vitro* experiments further proved that **DFlu** is able to sensitively visualize and monitor the dynamic changes of $ONOO^-$. Moreover, manipulation of $ONOO^-$ levels in adult

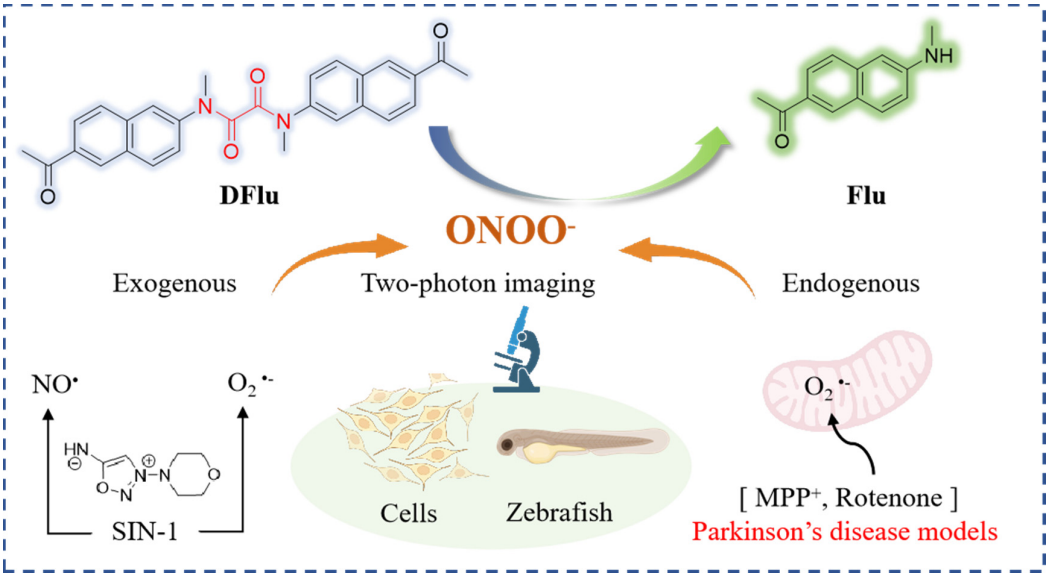

Scheme 1. Chemical structures and schematic illustration of **DFlu** for $ONOO^-$ detection in PD models (created with http://BioRender.com).

zebrafish could also be observed by two-photon imaging. These results might guide designing novel two-photon probes for $ONOO^-$ in multiple PD models.

2. Materials and Methods

2.1. *Materials and instrumentation*

All chemical reaction and cell imaging reagents were obtained from internet medicine suppliers without further purification unless otherwise noted. The progress in the chemical reaction and column chromatography was surveilled with thin-layer chromatography (TLC) on precoated silica plates (250 μm thickness), and the spots were observed with UV light. The nuclear magnetic resonance was recorded in Bruker ADVANCE NEO 500 spectrometer using $CDCl_3$ or d_6-DMSO at room temperature. U-3900H and F-7100, respectively, collected absorption and fluorescence data. High-performance liquid chromatography (HPLC) was performed on UltiMate 3000. A high-resolution mass spectrum was obtained by Micromass GCT-MS (ESI source).

2.2. *Preparation and Characterization*

1-(6-hydroxynaphthalen-2-yl)ethan-1-one (**A1**) and 1-(6-(methylamino)naphthalen-2-yl)ethan-1-one (**Flu**) were detailed described in detail in the experimental section of Supplementary Material. The date of ^{1}H NMR and ^{13}C NMR were shown in the Supporting Information.

2.2.1. *Preparation of 1-methyl-2,3-dioxo-2,3-dihydro-1H-benzo[f]indole-6-carbonitrile (SFlu)*

Oxalyl chloride (85.6 μL, 1 mmol) was added into 25 mL three-neck flask containing dry tetrahydrofuran (10 mL) in a nitrogen atmosphere. Subsequently, **Flu** (0.20 g, 1.00 mmol) was added dropwise and kept stirring for 4 h at 37°C. The product was collected by filtration to obtain red powder **SFlu** (0.21 g, 85%). ^{1}H NMR (500 MHz, d_6-DMSO) δ (ppm): 8.71 (s, 1H), 8.56 (d, J = 8.7 Hz, 1H), 8.48 (d, J = 8.7 Hz, 1H), 8.16 (d, J = 8.8 Hz, 1H), 7.62 (d, J = 8.7 Hz, 1H), 3.24 (s, 3H), 2.69 (s, 3H). ^{13}C NMR (126 MHz, d_6-DMSO) δ (ppm): 196.4, 182.3, 160.1, 157.6, 140.4, 133.4, 132.2, 130.9, 128.4, 121.9, 111.7, 108.3, 27.0, 26.7. $[M+H]^+$: calculated for 254.07, found 254.26.

2.2.2. *Preparation of N,N-bis(6-acetylnaphthalen-2-yl)-N1,N2-dimethyloxalamide (DFlu)*

Flu (0.20 g, 1.00 mmol) and K_2CO_3(0.70 g, 5.00 mmol) were added into 25 mL three-neck flask containing dry tetrahydrofuran (10 mL) at ice bath

conditions. After stirring for 10 min, oxalyl chloride (42.8 μL, 0.50 mmol) was added dropwise at 0°C. Then, the white suspension was observed and stirred at room temperature for 4 h. Using filtration, the product was obtained as a white powder (0.20 g, 90%). ^{1}H NMR (500 MHz, $CDCl_3$) δ (ppm): 8.51 (s, 2H), 8.11 (dd, J = 8.6, 1.7 Hz, 2H), 7.87 (d, J = 8.7 Hz, 2H), 7.70 (d, J = 8.5 Hz, 2H), 7.17 (d, J = 2.2 Hz, 2H), 6.90 (dd, J = 8.7, 2.2 Hz, 2H), 3.10 (s, 6H), 2.79 (s, 6H). ^{13}C NMR (126 MHz, $CDCl_3$) δ(ppm): 197.8, 164.8, 140.2,135.3, 131.2, 130.5, 129.6, 128.4, 125.3, 124.5, 123.7, 35.5, 26.8. $[M+H]^+$: calculated for 453.1736, found 453.1819.

2.3. *Absorption and fluorescence measurements*

The absorption and fluorescence were tested in phosphate buffer (1× PBS). **SFlu** and **DFlu** (1 mM) were dissolved in DMSO. The ion and amino acid (10 mM) was dissolved in deionized water. The fluorescence data were collected at 350 nm excitation wavelength with a 5 nm slit. A cytation 5 microplate reader recorded the stable response of the probe at different temperatures and pH.

2.4. *Cell culture and imaging*

SH-SY5Y cells were cultured in Dulbecco's modified medium (DMEM) containing 100 units/mL penicillin, 10% fetal bovine serum and 100 μg/mL streptomycin. When the cell density reaches 60–70% and maintains exponential growth, it is needed in several confocal dishes, and the cell density is observed to be around 60%. The cells are treated for imaging according to the requirements of different groups.

3-morpholinosydnonimine hydrochloride (SIN-1, 500 μM) was used to treat cells for 1 h at 37°C with or without the 4 h pretreatment of uric acid (UA, $ONOO^-$ scavenger, 200 μM) to image exogenous $ONOO^-$. To image endogenous $ONOO^-$ in PD models, 1-Methyl-4-Phenylpyridinium ion (500 μM) was applied to the cells for 4 h at 37°C with or without 4 h pretreatment of 200 μM UA. Subsequently, the cells were incubated with 10 μM **DFlu** for 1 h at 37°C, rinsed with PBS and imaged with Nikon confocal microscope.

2.5. *Zebrafish culture and imaging*

For exogenous $ONOO^-$ imaging, the five-day-old zebrafish were treated with 1 mM SIN-1 for 1 h with or without 4 h pretreatment of 500 μM UA. For endogenous $ONOO^-$ imaging in PD models, the zebrafish were treated with 3 mM MPP^+ for 2 h with or without 4 h pretreatment of 500 μM UA. Subsequently, **DFlu** were incubated for 3 h with zebrafish, rinsed with PBS and anesthetized with 0.01–0.02% tricaine prior to imaging. Zeiss LSM880 NLO Confocal Microscope was used for the imaging collection.

2.6. *Statistical analysis*

GraphPad Prism (GraphPad Software, San Diego, CA) was used to analyze all the experimental data. Normally distributed datasets were compared using a one-way ANOVA followed by Dunnet's *post-hoc* test where appropriate. A P-value of ≤ 0.05 was considered statistically significant. Data were expressed as mean ± SD.

3. Results and Discussion

3.1. *Design and synthesis*

To achieve high $ONOO^-$ selectivity, avoid autofluorescence interference and diminish light damage in living PD models during imaging, we chose the dicarbonyl group instead of aryldicarbonyl with a strong electron-withdrawing. Moreover, we utilize **Flu** as a two-photon-based fluorophore. **DFlu** was synthesized via the Stollé synthesis reaction between aldehyde oxalyl chloride and **Flu**. In the synthesis process, we found an interesting phenomenon: Oxalyl chloride is added in different orders to get different products (**DFlu** or **SFlu**), but both products contain α-ketoamide reactivity-based $ONOO^-$ recognition groups. To our best knowledge, the amide bond of the α-ketoamide group could be broken after reacting with nucleophilic $ONOO^-$ and then resulting in the change in fluorescence signals of **SFlu** and **DFlu**. Therefore, with the help of the fluorescence imaging technique can detect the dynamic changes of $ONOO^-$ in PD models. The detailed synthetic route is shown in Fig. S1. These compounds were well-validated through ^{1}H NMR, ^{13}C NMR and mass spectrometry.

3.2. *Spectroscopic response of probe to ONOO⁻*

The absorption spectra were first employed to determine the optimal reaction conditions between $ONOO^-$ and the probe to confirm the molecular design concept. The absorption spectra of **SFlu** and **DFlu** in different solvents were shown in Figs. S2 and S3, respectively. The absorption wavelength of **DFlu** was obviously changed only in DMSO because DMSO as an aprotic solvent may inhibit the generation of hydrogen bonds and improve the solubility of **DFlu** (Fig. S3).[40] Furthermore, the absorption spectra of **SFlu** and**DFlu** in the PBS/DMSO mixture solvent were tested (Figs. S4 and S5). When the ratios of DMSO and PBS are 8:2, the presence of 40 μM $ONOO^-$ modifies the absorption spectra of **SFlu** and **DFlu** dramatically. We next investigated the alteration in the absorption spectrum of **SFlu** and **DFlu** with various concentrations of $ONOO^-$ in the PBS/DMSO mixture solvent. As depicted in Fig. 1(a), the absorption spectra of **DFlu** gradually occurred as a new peak at 360 nm accompanied by the peak decline at 300 nm with a clear isosbestic point of 313 nm. In contrast, the absorption spectra of **SFlu** exhibited a noticeable hypochromic effect at 488 nm and a blue shift ranging from 480 nm to 412 nm [Fig. 1(b)]. The fluorescence titration experiments were shown in Fig. 1(b), and it demonstrated that **DFlu** displayed an apparent fluorescence turn-on changes at 490 nm. On the other hand, **SFlu** showed a fluorescence turn-off in the existance of $ONOO^-$ [Fig. 1(d)]. In order to reduce the background interference of the biological environment, the turn-on of fluorescence intensity of **DFlu** was selected for subsequent experiments.

We next investigated the sensitivity of **DFlu** for $ONOO^-$. In Fig. 1(e), the peak intensity at 490 nm increased gradually with increasing content of $ONOO^-$ and the detection limit of **DFlu** was calculated to be 9.89 nM. The rate constant of the reaction between the **DFlu** and $ONOO^-$ was further evaluated ($k = 0.0282\,\text{min}^{-1}$ at 37°C, Fig. S6 and Table S2), which is slower than that of α-ketoamide with strong electron absorption.[29] However, the change of fluorescence signal of **DFlu**

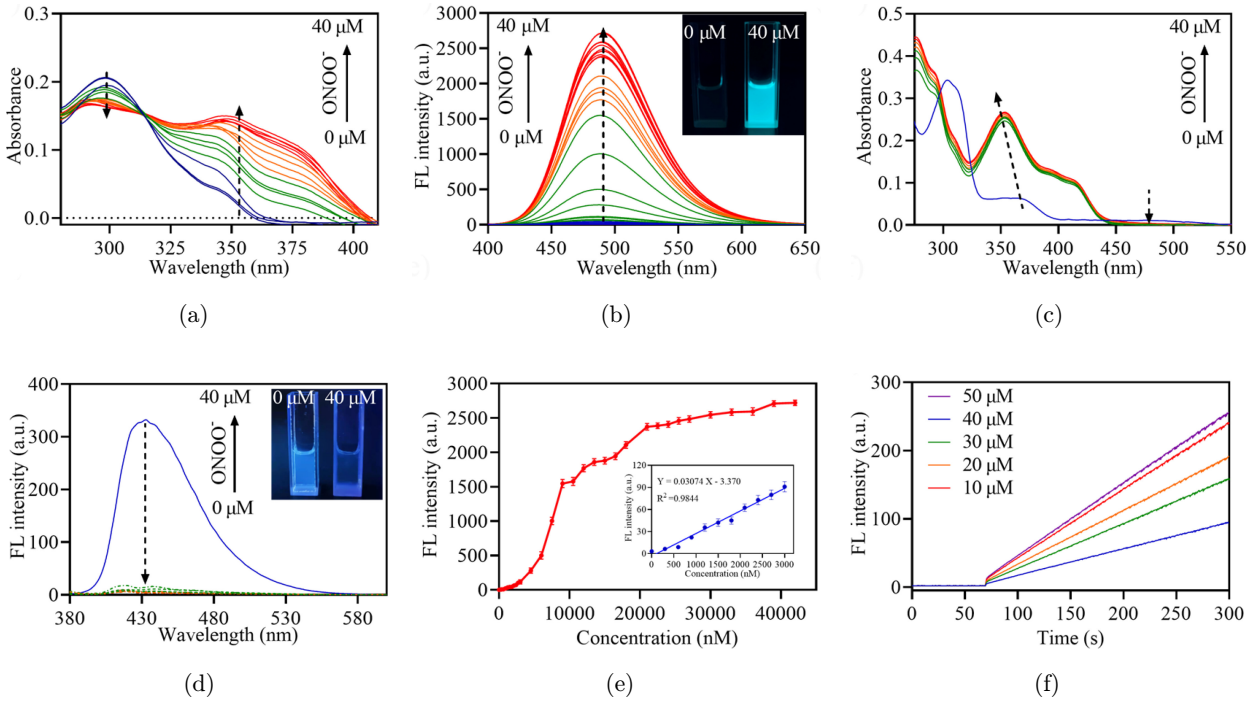

Fig. 1. (a) Absorption and (b) fluorescence spectra of **DFlu** (10 μM) toward various concentrations of $ONOO^-$ ($\lambda_{ex} = 350$ nm). (c) Absorption and (d) fluorescence spectra of **SFlu** (10 μM) with various concentrations of $ONOO^-$ ($\lambda_{ex} = 365$ nm). (e) The emission intensity change at 490 nm at the different concentrations of $ONOO^-$. Inset linear fitting curve of fluorescence intensity with different concentrations of $ONOO^-$ from 0 to 3000 nM. $\lambda_{ex} = 350$ nm, data represent mean ± SD ($n = 3$). (f) Fluorescence response of **DFlu** with the addition of $ONOO^-$. $ONOO^-$ was added at 60 s and fluorescence intensity at 490 nm was measured with excitation at 350 nm.

is obvious after reacting with $ONOO^-$ [Fig. 1(f)]. In addition, the **DFlu** and $ONOO^-$ reaction also had a yield of 64% (Fig. S7). These results indicated that **DFlu** is considered a powerful imaging tool to monitor $ONOO^-$ in the living system at low concentrations.

3.3. *Selective and stable response of DFlu towards ONOO⁻*

To test the specificity against $ONOO^-$, **DFlu** was tested with different anions (HCO_3^-; F^-; I^-; Br^-; NO_3^-; CO_3^{2-}; SO_4^{2-}), cations (Mg^{2+}; Al^{3+}; Cu^{2+}, Fe^{3+}; Mn^{2+}; Zn^{2+}; Ni^{2+}), amino acids (Glycine; Alanine; Valine; Methionine; Proline; Serine; Tyrosine; Histidine) and ROS ($ONOO^-$; ROO^-; $^1O_2$; ·OH; ClO^-; H_2O_2). As shown in Fig. 2(a), $ONOO^-$ was the only substance that enhanced the fluorescence of **DFlu**. In addition, the competitive experiments manifested that the fluorescence response of **DFlu** to $ONOO^-$ was not affected by other phycological substances [Fig. 2(b)]. Considering that $ONOO^-$ probes frequently cross-reacted with H_2O_2 due to their similar reactivity and peroxide moiety, high level of H_2O_2 was added to **DFlu** solution [Figs. 2(c) and 2(d)]. Inspiringly, no fluorescence increase was seen in the presence of 500 μM H_2O_2. Moreover, in the presence of biologically relevant reducing agents (GSH or CO_2), $ONOO^-$-dependent reactions are often altered.[41] $ONOO^-$ can be rapidly reduced by reductive reagents such as GSH and CO_2 which results in its short lifetime. However, **DFlu** is still able to detect $ONOO^-$ in a relatively short time [Figs. S8(a) and 8(b)], and as shown in Figs. S8(c) and 8(d), **DFlu** exhibited high sensitivity in the presence of high concentrations of GSH (100 μM) and CO_2 (12 mM), respectively. On the basis of these results, **DFlu** could selectively identify $ONOO^-$.[42,43]

In light of **DFlu** excellent anti-interference performance against $ONOO^-$, we further explore whether other biological environments, like temperature and pH, would affect the response signals. In Fig. 2(e), in the presence of 40 μM $ONOO^-$, the **DFlu** fluorescence intensity did not change significantly between 25°C and 45°C, indicating that **DFlu** monitoring $ONOO^-$ was not affected by temperature. Additionally, as shown in Fig. 2(f), **DFlu** exhibited weak fluorescence in the pH ranges from 4 to 10 without $ONOO^-$, and strong fluorescence intensity with $ONOO^-$ in pH of 6–8. The above results indicated that **DFlu** is suitable for detecting $ONOO^-$ in physiologically relevant conditions.

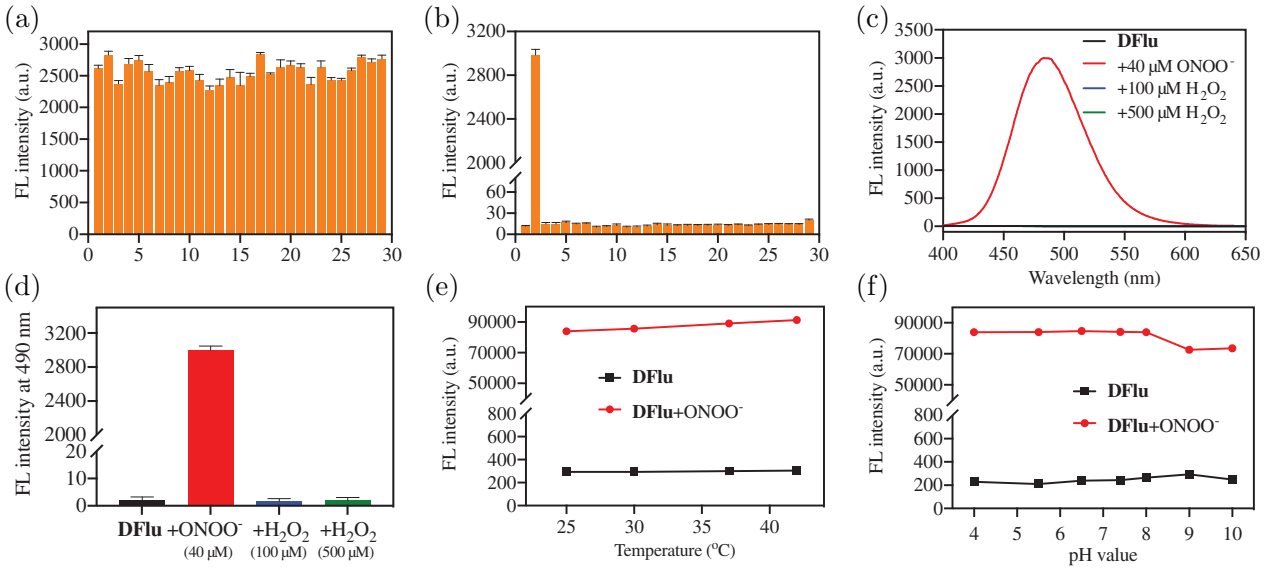

Fig. 2. (a) The fluorescence response of **DFlu** to various 1–29 substances: Blank; $ONOO^-$; ROO^-; $^1O_2$; ·OH; ClO^-; H_2O_2; Mg^{2+}; Al^{3+}; Cu^{2+}; Fe^{3+}; Mn^{2+}; Zn^{2+}; Ni^{2+}; HCO_3^-; F^-; I^-; Br^-; NO_3^-; CO_3^{2-}; SO_4^{2-}; Glycine; Alanine; Valine; Methionine; Proline; Serine; Tyrosine; Histidine. (b) Fluorescence intensity of **DFlu** reacting with $ONOO^-$ in the existence of 28 substances. λ_{ex} = 350 nm, λ_{em} = 490 nm, data represent mean ± SD (n = 3); (c) Fluorescence responses and (d) the columns plot of **DFlu** incubated with blank, H_2O_2 (100 μM), H_2O_2 (500 μM) and $ONOO^-$ (40 μM). The fluorescence intensity changes of 10 μM **DFlu** reaction with 40 μM $ONOO^-$ at (e) different temperatures and (f) different pH.

3.4. *Sensing mechanism of DFlu towards ONOO⁻*

Next, the mechanism of fluorescence signal activation of **DFu** was studied from both experimental and theoretical aspects. Firstly, the reaction between **DFlu** and $ONOO^-$ was confirmed by HPLC. The results displayed that the **Flu** (Rt = 3.34 min) was the main product after **DFlu** reacted with $ONOO^-$ [Fig. 3(a)]. In **Fig. S6**, high-resolution mass spectrometry (HR-MS) analysis further confirmed that the reaction produced **Flu** (m/z = 200.1076) is consistent with Scheme S1.

In order to further clarify the **DFlu** sensing mechanism, theoretical studies were conducted utilizing time-dependent DFT (TD-DFT) calculations at the B3LYP/6-31G (d) level using Gaussian 09. The results indicated that **DFlu** and **Flu** exhibited characteristic absorption peaks at 317 nm and 360 nm, respectively, which corresponded to experimental peaks at 345 nm and 354 nm [Figs. 3(b) and 3(c)]. In addition, the oscillator strengths (f) of **Flu** (f = 0.4349) is higher than **DFlu** (f = 0.1955), which corresponded to the high molar absorption coefficients of **Flu** compared to **DFlu** in Table S3. Moreover, the frontier molecular orbitals play crucial roles in the electronic transition. As shown in Fig. 3(d), the electrons of the highest occupied molecular orbital (HOMO) and the lowest unoccupied molecular orbital (LUMO) were independently distributed at the ends of **DFlu**, implying that the amide bonds have suppressed the push–pull electron effect of **DFlu**. Conversely, the electrons on HOMO and LUMO were mainly distributed throughout the entire molecule, which indicated the amide bond was cleaved and produced **Flu** with a strong fluorescence signal due to the recovery of ICT. Furthermore, as shown in Table S3 and Fig. S9, the high quantum yield (0.918) and emission wavelength redshift with increasing polarity of **Flu** also shows that the strong fluorescence originates from the nature of ICT. Moreover, the HOMO–LUMO energy gap was 3.6462–3.4944 eV, which is consistent with the apparent redshift in the absorption spectrum after reactions between **DFlu** reacting with $ONOO^-$.

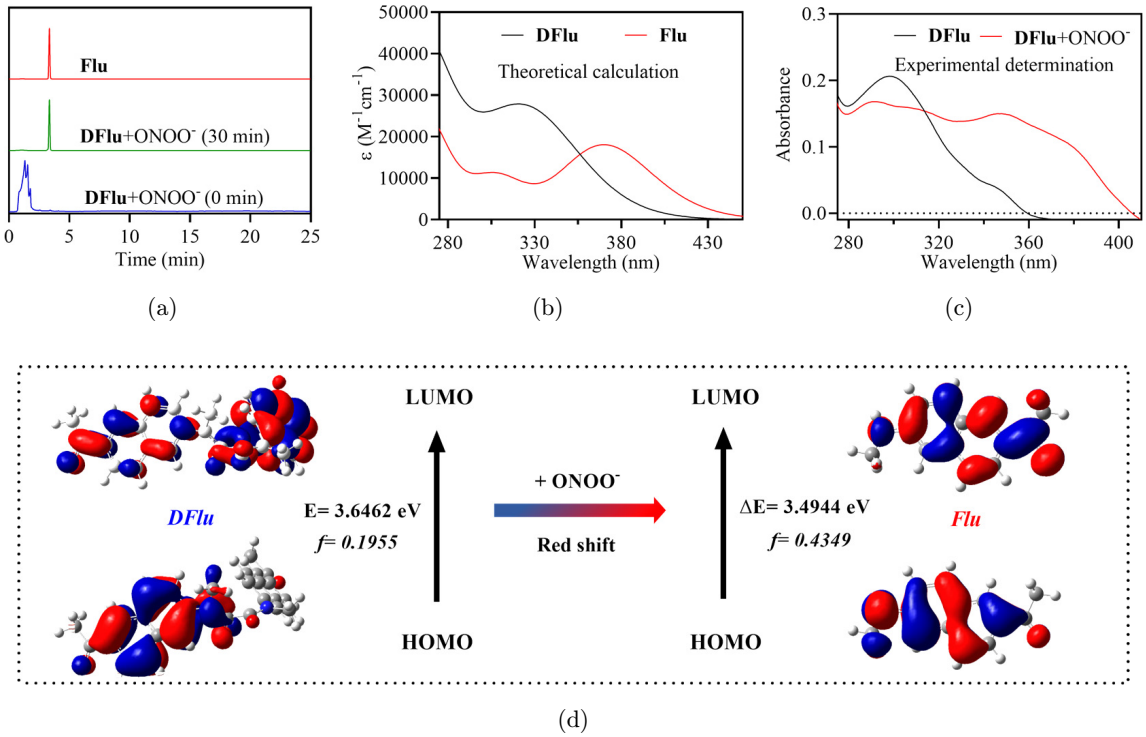

Fig. 3. (a) The HPLC changes of **DFlu** reacting with $ONOO^-$ for 30 min. (b) The theoretical TDDFT absorption peak **DFlu** and **Flu**; (c) The experimental absorption peak of **DFlu** with and without $ONOO^-$; (d) The DFT optimization of the structures and frontier molecular orbitals for **DFlu** and **Flu**.

3.5. *The imaging of ONOO⁻ in living cells*

Based on the excellent fluorescent response of **DFlu** to $ONOO^-$, we attempted to utilize **DFlu** to visualize the $ONOO^-$ in living cells. Before cell imaging, we evaluated the cytotoxicity of different **DFlu** concentrations. After being treated with 20 μM **DFlu** for 24 h, the viability of SH-SY5Y cells and RAW 264.7 cells remained above 80% (Fig. S10). Next, **DFlu** was employed to monitor the exogenous and endogenous $ONOO^-$. For the exogenous $ONOO^-$ imaging, we stimulated SH-SY5Y cells with SIN-1 ($ONOO^-$ donor). As shown in Figs. 4(a) and 4(b), no fluorescence signals were observed in **DFlu**-treated cells. However, the cells exhibited significant fluorescence increase SIN-1 stimulation. After being pretreated with UA ($ONOO^-$ scavenger), the fluorescence signal intensity induced by SIN-1 was distinctly diminished. These results reveal that **DFlu** possesses the capability to monitor exogenous $ONOO^-$.

Furthermore, we used MPP^+, an acute clinical parkinsonism inductive agent, to reveal the variation of $ONOO^-$ in PD disease at the cellular level.[44] After treating with MPP^+ for 8 h, a noticeable boost in fluorescence intensity was observed [Fig. 4(c)]. Meanwhile, when a combination of MPP^+ and UA was used to treat cells, no remarkable increased fluorescence was observed [Fig. 4(d)]. In addition, we also used **DFlu** to monitor $ONOO^-$ levels in rotenone-induced PD models and obtained the same fluorescence imaging results (Fig. S11). Moreover, we observed that the $ONOO^-$ levels were slightly lower in the rotenone-induced PD model than in the MPP^+-induced PD model. Meanwhile, **DFlu** successfully detected excessive $ONOO^-$ levels in inflammatory models (Fig. S12). These results further proved that **DFlu** could detect the exogenous and endogenous $ONOO^-$ levels *in vitro* and serve as a promising molecular imaging tool to visualize abnormal $ONOO^-$ levels under pathological conditions.

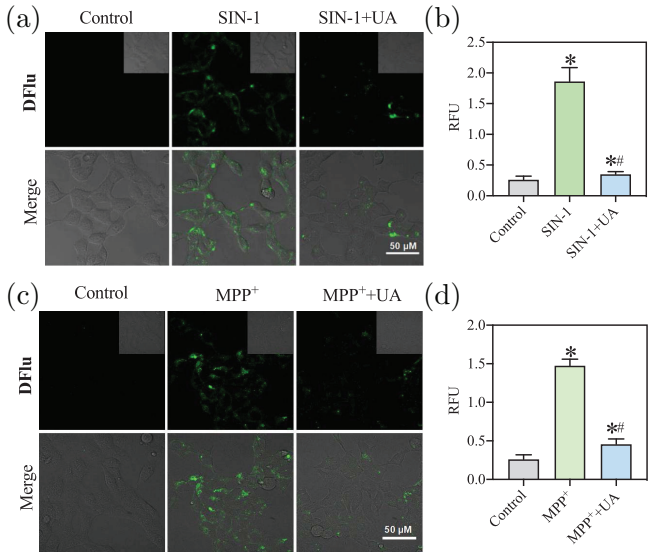

Fig. 4. Confocal bioimaging of $ONOO^-$ levels. (a) and (c) Representative images of SH-SY5Y cells treated with **DFlu** (10 μM, 1 h) after SIN-1 or MPP^+ treatment. Scale bar = 50 μm. $\lambda_{ex} = 405$ nm, $\lambda_{em} = 500$–570 nm. (b) and (d) The fluorescence intensity was quantified and the data were expressed as mean ± SD ($n = 3$). $^*P < 0.05$ versus control, $^\#P < 0.05$ versus SIN-1 or MPP^+.

3.6. *The imaging of ONOO⁻ in zebrafish*

Encouraged by the capability of the probe to visualize exogenous/endogenous $ONOO^-$ and the excellent two-photon properties of the product (**Flu**) after the reaction between **DFlu** and $ONOO^-$ (Fig. S13), we further investigated whether **DFlu** could be applied for visualizing $ONOO^-$ levels *in vivo* by two-photon confocal microscope. As shown in Figs. 5(a) and 5(b), the SIN-1 treated zebrafish using exogenous $ONOO^-$ models exhibited strong

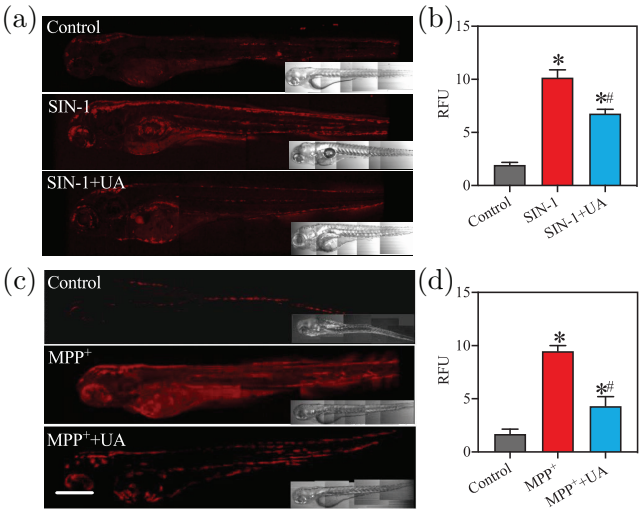

Fig. 5. Two-photon fluorescence bioimaging of $ONOO^-$ levels in zebrafish. (a) and (c) Representative images of living zebrafish upon incubation with **DFlu** (10 μM, 3 h) after SIN-1 or MPP^+ treatment. Scale bar = 200 μm, $\lambda_{ex} = 760$ nm, $\lambda_{em} = 420$–500 nm. (b) and (d) The fluorescence intensity was quantified and the data were expressed as mean ± SD ($n = 3$). $^*P < 0.05$ versus control, $^\#P < 0.05$ versus SIN-1 or MPP^+.

TP fluorescence compared to the control and SIN-1 +UA groups. Moreover, the MPP^+-treated zebrafish were used as PD disease models. As shown in Figs. 5(c) and 5(d), strong red two-photon fluorescence was observed when the MPP^+-treated zebrafish was incubated with **DFlu** for 3 h. Furthermore, the recorded fluorescence signal decreased significantly in the presence of UA. In addition, the same results were obtained in the zebrafish model of PD induced by rotenone (Fig. S14). These results demonstrated that **DFlu** could accurately discriminate the area with high levels of $ONOO^-$ in the zebrafish PD model.

4. Conclusion

In conclusion, we developed novel α-ketoamide recognition moieties and used it to construct a two-photon peroxynitrite probe (**DFlu**). The conspicuous fluorescence of **DFlu** at 490 nm was observed to be stimulated by $ONOO^-$ and the theoretical calculation showed strong fluorescence from the recovery of ICT capacity. **DFlu** exhibited good stability and excellent selectivity in the presence of other reactive substances. In addition, **DFlu** could detect exogenous and endogenous $ONOO^-$ in living cells with negligible cytotoxicity. More importantly, **DFlu** could detect endogenous/exogenous $ONOO^-$ in PD zebrafish models by two-photon imaging. These results could guide the design of the probe's red-shifting absorption and emission based on push and pull electrons and could promote a new way to construct α-ketoamide-based two-photon $ONOO^-$ probes for the in-depth study of $ONOO^-$ stress-related diseases.

Conflict of Interest

The authors declare that there are no conficts of interest relevant to this article.

Acknowledgments

This work was financially supported by the National Natural Science Foundation of China (22077101), the Open Project Program of Wuhan National Laboratory for Optoelectronics (No. 2020WNLOKF023), Natural Science Foundation of Shaanxi Province (2022JM-130), the Joint Research Funds of Department of Science & Technology of Shaanxi Province and Northwestern Polytechnical University (2020GXLH-Z-008, 2020GXLH-Z-021, 2020GXLH-Z-023), the China Postdoctoral Science Foundation (2022M711595, 2022M722595), Postdoctoral Research Funding Schemes of Jiangsu Province (2021K036A), The Natural Science Foundation of Ningbo (202003N4049, 202003N4065). Tao Shao and Xianning Xu contributed equally to this work.

References

1. W. Dauer, S. Przedborski, "Parkinson's disease: Mechanisms and models," *Neuron* **39**, 889–909 (2003).
2. L. Gao, W. Wang, X. Wang, F. Yang, L. Xie, J. Shen, M. A. Brimble, Q. Xiao, S. Q. Yao, "Fluorescent probes for bioimaging of potential biomarkers in Parkinson's disease," *Chem. Soc. Rev.* **50**, 1219–1250 (2021).
3. J. S. Paulsen, M. Nance, J. I. Kim, N. E. Carlozzi, P. K. Panegyres, C. Erwin, A. Goh, E. McCusker, J. K. Williams, "A review of quality of life after predictive testing for and earlier identification of neurodegenerative diseases," *Prog. Neurobiol.* **110**, 2–28 (2013).
4. W. Poewe, K. Seppi, C. M. Tanner, G. M. Halliday, P. Brundin, J. Volkmann, A. E. Schrag, A. E. Lang, "Parkinson disease," *Nat. Rev. Dis. Primers* **3**, 17013 (2017).
5. A. Wood-Kaczmar, S. Gandhi, N. W. Wood, "Understanding the molecular causes of Parkinson's disease," *Trends Mol. Med.* **12**, 521–528 (2006).
6. M. J. Armstrong, M. S. Okun, "Diagnosis and treatment of Parkinson disease: A review," *JAMA* **323**, 548–560 (2020).
7. S. G. Reich, J. M. Savitt, "Parkinson's disease," *Med. Clin. North Am.* **103**, 337–350 (2019).
8. D. Nemade, T. Subramanian, V. Shivkumar, "An update on medical and surgical treatments of parkinson's disease," *Aging Dis* **12**, 1021–1035 (2021).
9. M. Weng, X. Xie, C. Liu, K. L. Lim, C. W. Zhang, L. Li, "The sources of reactive oxygen species and its possible role in the pathogenesis of Parkinson's disease," *Parkinson's Dis.* **2018**, 9163040 (2018).
10. K. H. Chang, C. M. Chen, "The role of oxidative stress in Parkinson's disease," *Antioxidants* **9**, 597 (2020).
11. L. Huang, Z. Sun, Q. Shen, Z. Huang, S. Wang, N. Yang, G. Li, Q. Wu, W. Wang, L. Li, C. Yu, "Rational design of nanocarriers for mitochondria-targeted drug delivery," *Chin. Chem. Lett.* **33**, 4146–4156 (2022).

12. K. J. Barnham, C. L. Masters, A. I. Bush, "Neurodegenerative diseases and oxidative stress," *Nat. Rev. Drug Discov.* **3**, 205–214 (2004).
13. W. L. Cui, M. H. Wang, Y. H. Yang, J. Y. Wang, X. Zhu, H. Zhang, X. Ji, "Recent advances and perspectives in reaction-based fluorescent probes for imaging peroxynitrite in biological systems," *Coord. Chem. Rev.* **474**, 214848 (2023).
14. Z. Mao, J. Xiong, P. Wang, J. An, F. Zhang, Z. Liu, J. Seung Kim, "Activity-based fluorescence probes for pathophysiological peroxynitrite fluxes," *Coord. Chem. Rev.* **454**, 214356 (2022).
15. V. K. Pandey, P. J. Amin, B. S. Shankar, "G1-4A, a polysaccharide from tinospora cordifolia induces peroxynitrite dependent killer dendritic cell (KDC) activity against tumor cells," *Int. Immunopharmacol.* **23**, 480–488 (2014).
16. P. Michalska, R. León, "When it comes to an end: Oxidative stress crosstalk with protein aggregation and neuroinflammation induce neurodegeneration," *Antioxidants* **9**, 740 (2020).
17. H. Kang, W. Shu, J. Yu, M. Gao, R. Han, J. Jing, R. Zhang, X. Zhang, "A near-infrared fluorescent probe for ratiometric imaging peroxynitrite in Parkinson's disease model," *Sens. Actuators B, Chem.* **359**, 131393 (2022).
18. Q. Sun, J. Xu, C. Ji, M. S. S. Shaibani, Z. Li, K. Lim, C. Zhang, L. Li, Z. Liu, "Ultrafast detection of peroxynitrite in Parkinson's disease models using a near-infrared fluorescent probe," *Anal. Chem.* **92**, 4038–4045 (2020).
19. B. J. Bezner, L. S. Ryan, A. R. Lippert, "Reaction-based luminescent probes for reactive sulfur, oxygen, and nitrogen species: Analytical techniques and recent progress," *Anal. Chem.* **92**, 309–326 (2020).
20. A. Grzelakowska, J. Modrzejewska, J. Kolińska, M. Szala, M. Zielonka, K. Dębowska, M. Zakłos-Szyda, A. Sikora, J. Zielonka, R. Podsiadły, "Water-soluble cationic boronate probe based on coumarin imidazolium scaffold: Synthesis, characterization, and application to cellular peroxynitrite detection," *Free Radic. Biol. Med.* **179**, 34–46 (2022).
21. H. Kobayashi, M. Ogawa, R. Alford, P. L. Choyke, Y. Urano, "New strategies for fluorescent probe design in medical diagnostic imaging," *Chem. Rev.* **110**, 2620–2640 (2010).
22. F. Wang, X. Jiang, H. Xiang, N. Wang, Y. Zhang, X. Yao, P. Wang, H. Pan, L. Yu, Y. Cheng, Y. Hu, W. Lin, X. Li, "An inherently kidney-targeting near-infrared fluorophore based probe for early detection of acute kidney injury," *Biosens. Bioelectron.* **172**, 112756 (2021).
23. L. Zhang, Y. Liu, H. Huang, H. Xie, B. Zhang, W. Xia, B. Guo, "Multifunctional nanotheranostics for near infrared optical imaging-guided treatment of brain tumors," *Adv. Drug Deliv. Rev.* **190**, 114536 (2022).
24. Y. Liu, D. Zhuang, J. Wang, H. Huang, R. Li, C. Wu, Y. Deng, G. Hu, B. Guo, "Recent advances in small molecular near-infrared fluorescence probes for a targeted diagnosis of the Alzheimer disease," *Analyst* **147**, 4701–4723 (2022).
25. I. Hasan, B. Guo, J. Zhang, C. Chang, "Advances in antioxidant nanomedicines for imaging and therapy of Alzheimer's disease," *Antioxidants Redox Signal.* (2022), doi.org/10.1089/ars.2022.0107.
26. Y. Zuo, X. Wang, W. Lin, "Four-armed functional siloxane enables ratiometric unconventional fluorescence for the detection of $ONOO^-$," *Sens. Actuat. B. Chem.* **331**, 129462 (2021).
27. J. Cui, S. Zang, H. Nie, T. Shen, S. Su, J. Jing, X. Zhang, "An ICT-based fluorescent probe for ratiometric monitoring the fluctuations of peroxynitrite in mitochondria," *Sens. Actuators B, Chem.* **328**, 129069 (2021).
28. C. Ling, M. Cui, J. Chen, L. Xia, D. Deng, Y. Gu, P. Wang, "A novel highly selective fluorescent probe with new chalcone fluorophore for monitoring and imaging endogenous peroxynitrite in living cells and drug-damaged liver tissue," *Talanta* **215**, 120934 (2020).
29. D. Cheng, W. Xu, L. Yuan, X. Zhang, "Investigation of drug-induced hepatotoxicity and its remediation pathway with reaction-based fluorescent probes," *Anal. Chem.* **89**, 7693–7700 (2017).
30. Y. Li, X. Xie, X. E. Yang, M. Li, X. Jiao, Y. Sun, X. Wang, B. Tang, "Two-photon fluorescent probe for revealing drug-induced hepatotoxicity via mapping fluctuation of peroxynitrite," *Chem. Sci.* **8**, 4006–4011 (2017).
31. X. Xie, X. E. Yang, T. Wu, Y. Li, M. Li, Q. Tan, X. Wang, B. Tang, "Rational design of an α-ketoamide-based near-infrared fluorescent probe specific for hydrogen peroxide in living systems," *Anal. Chem.* **88**, 8019–8025 (2016).
32. W. Qu, C. Niu, X. Zhang, W. Chen, F. Yu, H. Liu, X. Zhang, S. Wang, "Construction of a novel far-red fluorescence light-up probe for visualizing intracellular peroxynitrite," *Talanta* **197**, 431–435 (2019).
33. L. Li, C. W. Zhang, G. Y. J. Chen, B. Zhu, C. Chai, Q. H. Xu, E. K. Tan, Q. Zhu, K. L. Lim, S. Q. Yao, "A sensitive two-photon probe to selectively detect monoamine oxidase B activity in Parkinson's disease models," *Nat. Commun.* **5**, 3276 (2014).
34. M. Yan, H. Fang, X. Wang, J. Xu, C. Zhang, L. Xu, L. Li, "A two-photon fluorescent probe for visualizing endoplasmic reticulum peroxynitrite in Parkinson's disease models," *Sens. Actuators B, Chem.* **328**, 129003 (2021).

35. Z. Fang, Z. Su, W. Qin, H. Li, B. Fang, W. Du, Q. Wu, B. Peng, P. Li, H. Yu, L. Li, W. Huang, "Two-photon dual-channel fluorogenic probe for in situ imaging the mitochondrial H_2S/viscosity in the brain of drosophila Parkinson's disease model," *Chin. Chem. Lett.* **31**, 2903–2908 (2020).
36. B. C. Dickinson, C. J. Chang, "A targetable fluorescent probe for imaging hydrogen peroxide in the mitochondria of living cells," *J. Am. Chem. Soc.* **130**, 9638–9639 (2008).
37. G. Zhang, Z. Li, F. Chen, D. Zhang, W. Ji, Z. Yang, Q. Wu, C. Zhang, L. Li, W. Huang, "A novel fluorogenic probe for visualizing the hydrogen peroxide in Parkinson's disease models," *J. Innov. Opt. Health Sci.* **13**, 2050013 (2020).
38. X. Qiu, C. Xin, W. Qin, Z. Li, D. Zhang, G. Zhang, B. Peng, X. Han, C. Yu, L. Li, W. Huang, "A novel pyrimidine based deep-red fluorogenic probe for detecting hydrogen peroxide in Parkinson's disease models," *Talanta* **199**, 628–633 (2019).
39. H. Li, C. Xin, G. Zhang, X. Han, W. Qin, C. W. Zhang, C. Yu, S. Jing, L. Li, W. Huang, "A mitochondria-targeted two-photon fluorogenic probe for the dual-imaging of viscosity and H_2O_2 levels in Parkinson's disease models," *J. Mater. Chem. B* **7**, 4243–4251 (2019).
40. M. Li, X. Gong, H. W. Li, H. Han, S. Shuang, S. Song, C. Dong, "A fast detection of peroxynitrite in living cells," *Anal. Chim. Acta* **1106**, 96–102 (2020).
41. A. Sikora, J. Zielonka, M. Lopez, J. Joseph, B. Kalyanaraman, "Direct oxidation of boronates by peroxynitrite: Mechanism and implications in fluorescence imaging of peroxynitrite," *Free Rad. Biol. Med.* **47**, 1401–1407 (2009).
42. F. Yu, P. Li, B. Wang, K. Han, "Reversible near-infrared fluorescent probe introducing tellurium to mimetic glutathione peroxidase for monitoring the redox cycles between peroxynitrite and glutathione *in vivo*," *J. Am. Chem. Soc.* **135**, 7674–7680 (2013).
43. F. Yu, P. Li, G. Li, G. Zhao, T. Chu, K. Han, "A near-IR reversible fluorescent probe modulated by selenium for monitoring peroxynitrite and imaging in living cells," *J. Am. Chem. Soc.* **133**, 11030–11033 (2011).
44. V. S. Van Laar, J. Chen, A. D. Zharikov, Q. Bai, R. Di Maio, A. A. Dukes, T. G. Hastings, S. C. Watkins, J. T. Greenamyre, C. M. St Croix, E. A. Burton, "α-synuclein amplifies cytoplasmic peroxide flux, oxidative stress provoked by mitochondrial inhibitors in CNS dopaminergic neurons *in vivo*," *Redox Biol.* **37**, 101695 (2020).